Bi Adsorption and Poisoning on Ni(100) Surface As Probed by CO Chemisorption†

ARTICLE · MARCH 2000

DOI: 10.1021/jp992874h

Bi Adsorption and Poisoning on Ni(100) Surface As Probed by CO Chemisorption†

Chameli Panja, Mark E. Jones,‡ John M. Heitzinger,§ Steven C. Gebhard,|| and Bruce E. Koel*

Department of Chemistry, University of Southern California, Los Angeles, California 90089-0482

Received: August 13, 1999; In Final Form: November 30, 1999

CO chemisorption on Bi-modified Ni(100) surfaces, along with the structure and growth of vapor-deposited Bi adlayers on Ni(100), was characterized by Auger electron spectroscopy (AES), temperature-programmed desorption (TPD), low-energy electron diffraction (LEED), energy loss spectroscopy (ELS), UV photoelectron spectroscopy (UPS), work function measurements, and high-resolution electron energy loss spectroscopy (HREELS). Bi growth on Ni(100) at 500 K proceeds via a layer-plus-island (Stranski−Krastanov) growth mode and the gradual formation of a $c(2 \times 2)$ structure near monolayer coverage. Desorption of Bi from the first monolayer on Ni(100) occurs with an activation energy $E_d = 290-240$ kJ mol^{-1}. Bi desorption from Bi multilayers has $E_d = 200$ kJ mol^{-1}. Adsorbed Bi changed the work function of the Ni(100) surface only slightly, indicating an initial dipole moment of only −0.5 D and thus relatively little charge transfer between Bi and Ni compared to other modifier adlayers. CO chemisorption was used to probe the reactivity of Ni(100) surfaces modified by preadsorbed Bi adlayers, denoted as Bi/Ni(100). Only a small decrease (4 kJ mol^{-1}) occurs for the CO adsorption energy as determined by CO TPD. Site-blocking effects dominate over electronic (ligand) effects on the surface chemistry of CO on Bi/Ni(100). A comparison of these results to those on Bi/Pt(111), where Bi has been used as a model inert site-blocking agent, indicates that Bi modifies the electronic structure of Ni(100) even less than on Pt(111). Therefore, Bi adatoms may allow useful probing of adsorption and reaction ensemble requirements on Ni surfaces that contain modifiers as adatoms.

1. Introduction

The chemical and physical properties of bimetallic surfaces are central to a variety of technologically important areas including catalysis, superconductivity, electronics, and tribology. Thin films of Bi are of increasing interest for possible applications in semiconductor devices[1,2] and in fabrication of high-temperature superconductors.[3,4] Accordingly, several surface science investigations of Bi adsorption on various metal substrates have been reported.[5−9]

In addition, Bi adatoms on Pt surfaces have been shown to be useful in probing fundamental questions in catalysis.[10,11] This relates to continuing efforts to identify the origins of the often large effects of a second metal component in bimetallic catalysts. These effects are usually attributed to either electronic (ligand) or geometric (ensemble) effects on adsorption and reaction rates.[12,13] The difficulty in distinguishing between these two effects and establishing their relative importance, of course, depends on finding model systems that can be used to separate these two effects. There are certain advantages in using Bi as a model site-blocking agent: (i) it is relatively inert for activating or dissociating adsorbates in surface reactions, only physisorbing most molecules; (ii) the electronegativity difference is small between Bi and metals that are of interest as catalysts, such as Pt, Pd, and Ni, implying that only a small charge transfer may occur between the substrate and Bi overlayer. Bi and these metals do not readily form alloys, again indicating weak interactions.[10,11]

We have investigated CO chemisorption as a probe of the reactivity of Bi/Ni(100) surfaces primarily using a combination of temperature-programmed desorption (TPD) and high-resolution electron energy-loss spectroscopy (HREELS). We also performed Auger electron spectroscopy (AES), low-energy electron diffraction (LEED), UV photoelectron spectroscopy (UPS), and energy loss spectroscopy (ELS) studies to further characterize the growth mode and structure of vapor-deposited films of Bi on Ni(100), complementing earlier reports on the growth[7] and thermal desorption[14] of Bi on Ni(100). We found that adsorbed Bi causes only minimal chemical perturbations in CO−Ni(100) bonding and mainly physically blocks chemisorption sites on the Ni substrate. Bi−Bi repulsive interactions cause the Bi adatoms to be relatively dispersed on Ni(100). The combination of weak electronic interactions and repulsive lateral interactions makes the Bi/Ni(100) system useful for studies of Ni surface modification and probing ensemble effects in chemisorption and catalysis on Ni.

2. Experimental Section

These experiments were performed in an ultrahigh vacuum (UHV) chamber with a base pressure of 4×10^{-11} Torr, which has been previously described.[15] Briefly, it was equipped with a double-pass cylindrical mirror analyzer (CMA) for AES and a quadrupole mass analyzer (UTI 100 C) under computer control for TPD. The sample temperature was controlled by a linear ramp generator using a chromel−alumel thermocouple spot-welded to the crystal.

A polished Ni(100) single crystal was used. The Ni(100) crystal was cleaned at 500 K by ion sputtering with 500 eV Ar^+ ions and then annealed to 1400 K in UHV for 60 s. Surface purity was confirmed using AES and LEED. Contamination by sulfur, oxygen, and carbon was removed by oxidation at 1000

† Part of the special issue "Gabor Somorjai Festschrift".

* To whom correspondence should be addressed.
‡ Dow Chemical Company, 1776 Building, Midland, MI 48674.
§ FSI International, 322 Lake Hazeltine Drive, Chaska, MN 55318.
|| TDA Research Inc. 12345 West 52 Avenue, Wheat Ridge, CO 80033.

10.1021/jp992874h CCC: $19.00
Published on Web 03/02/2000

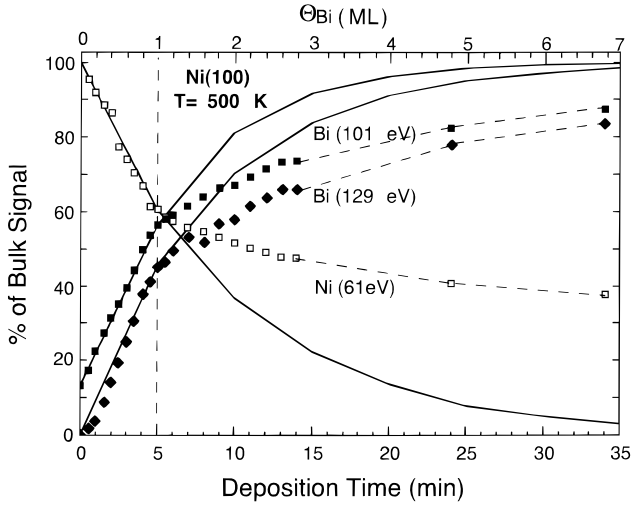

Figure 1. Changes in AES signal intensity during Bi deposition on a Ni(100) crystal at 500 K. The Bi monolayer coverage along the top axis is defined as $\Theta_{Bi} = 1$ or 8.05×10^{14} atoms cm^{-2}. The solid lines were calculated for a Bi layer-by-layer growth mode using the Ni and Bi AES signal intensities at $\Theta_{Bi} = 1$. The dashed lines are only a guide for the eye.

K in 5×10^{-9} Torr of O_2 for 60 s, followed by reduction in 1×10^{-8} Torr of H_2 at 1200 K for 30−60 s and then heating in UHV to 1400 K.

Bismuth (5 N purity) was deposited on the clean Ni(100) surface by means of a collimated thermal evaporation source. The dose rate was estimated to be 3×10^{12} atoms cm^{-2} s^{-1}. The power applied to the Bi evaporator was monitored to ensure reproducible dosing rates. The saturation Bi monolayer coverage was defined to be $\Theta_{Bi} = 1.0$ for 8.05×10^{14} Bi atoms cm^{-2}.[7] The term saturation monolayer is used to refer to a Bi adlayer that is one atom thick in which all Bi atoms are directly bound to the Ni substrate. The underlying Ni(100) substrate has a surface atom density of 1.61×10^{15} atoms cm^{-2}. Equivalent Bi coverages could be formed both by direct deposition and by annealing thick films.

CO exposures were carried out using a leak valve connected to a multichannel array doser. CO (Matheson, 99.5% purity) gas was used without further purification.

UPS spectra were obtained with a −10 V potential applied to the sample to offset the onset of secondary emission from zero kinetic energy. He(I) ($\hbar\omega = 21.22$ eV) UPS spectra were recorded using the CMA at a resolution of 300 meV. The incident UV light was at an angle $\Theta = 42.5°$ from the crystal normal. HREELS spectra were taken with a spectrometer containing single 127° cylindrical sectors in the monochromator and analyzer. All spectra were taken in specular reflection with $\Theta_{in} = \Theta_{out} = 65°$ from the surface normal. The electron incident energy was 4.5 eV, and the typical resolution was 80 cm^{-1}.

3. Results

3.1. Bi Adsorption and Initial Growth of Bi Films on Ni(100). *AES Studies.* The deposition and initial growth mechanism of Bi adlayers and ultrathin films on Ni(100) were characterized by AES using the peak-to-peak heights of the Ni(61 eV), Ni(848 eV), Bi(101 eV), and Bi(129 eV) Auger signals as a function of Bi deposition time. An Auger "uptake" plot of AES intensities versus Bi deposition time on Ni(100) at 500 K is shown in Figure 1. The Bi(101 eV) intensity was not zero at zero Bi coverage because of a low-intensity Ni(101 eV) transition[16] that is coincident with the Bi transition. But, the stronger Bi signal quickly overwhelmed the small Ni 101 eV signal, which was also attenuated by the Bi overlayer. We concurrently monitored the Bi(129 eV) transition to confirm that ignoring the Ni interference at 101 eV kinetic energy does not cause a major problem. The Bi and Ni curves shown in Figure 1 exhibit a pronounced change in slope ("break") at a deposition time near 5 min. No other such breaks in the curves was observed unambiguously. For a layer-by-layer (Frank−van der Merwe or FM) growth mechanism, the intensity values at the monolayer break point can be used to calculate the shape of the entire uptake curve.[17] Such curves are shown as solid lines in Figure 1. Deviations of the AES data from the calculated FM curves rule out a layer-by-layer mechanism for the growth of Bi films on Ni(100) at 500 K. Rather, the AES uptake curves are indicative of nucleation and growth of 3D Bi islands after completion of a Bi monolayer, i.e., Stranski−Krastanov (SK) growth.[18,19] Such uptake behavior could also indicate interdiffusion or alloying of Bi and Ni, but this does not occur extensively (vida infra).

Calculation of λ, the electron inelastic mean free path (IMFP), at 61 eV kinetic energy using the attenuation of the Ni(61 eV) signal during the Bi monolayer formation and $d_{100}(\text{Bi}) = 3.09$ Å[20] yields a value of $\lambda = 11.2$ Å. This is much higher than the expected value of 4.2 Å from the "universal curve",[21] but this disagreement is not too surprising. IMFPs calculated from the universal curve are most inaccurate in the region of 50−150 eV kinetic energy and ignores the well-documented dependence of IMFPs on the material.[22] Raw data used in formulating the universal curve show similar IMFPs at this energy.[21] Calculated IMFPs in Bi are also significantly larger than the values calculated in transition metals.[22] In addition, several assumptions were used for the mean free path calculations that introduce error. Most serious of these assumptions are that the densities of the substrate and adsorbate are equal.[23] The size difference between Bi and Ni requires that the Bi monolayer formed initially must be less dense than the Ni substrate.

The initial stages of Bi film growth were studied at four different Ni substrate temperatures, as shown in Figure 2. The Ni(61 eV) signal was most sensitive to changes in the growth mode because of the shorter mean free path at this energy. The attenuation of the Ni signal was greater at 150 K than at 500 K, which means that the average Bi islands thickness increased with temperature. The Bi(101 eV) signal was quite insensitive to the Ni(100) substrate temperature during deposition. When Bi films that had been deposited at low temperatures were annealed to 500 K, AES signals were produced that were identical to those obtained by Bi deposition on the substrate at 500 K. Heating the Ni(100) crystal to 750 K following any initial Bi coverage exceeding one monolayer ($\Theta_{Bi} > 1$) produced Bi and Ni AES intensities identical to those observed at the monolayer break point.

Figure 3 shows the results of annealing experiments probing the thermal stability of Bi thin films for three initial Bi coverages deposited on Ni(100) at 150 K. The Ni(61 eV) substrate signal for $\Theta_{Bi}^{init} = 0.6$ is nearly constant until 1050 K. At higher temperatures, the Ni(61 eV) signal was independent of the initial Bi coverage used and increased toward the value for clean Ni. The Ni(61 eV) signal for $\Theta_{Bi}^{init} = 1.0$ was constant up to 800 K. After a small decrease, possibly due to ordering changes in the Bi adlayer, the signal increases above 900 K and reaches the clean Ni value at 1250 K. In contrast to the two other curves, the Ni(61 eV) intensity after $\Theta_{Bi}^{init} = 2.2$ increases between 150 and 400 K. The Ni signal is relatively constant between 400

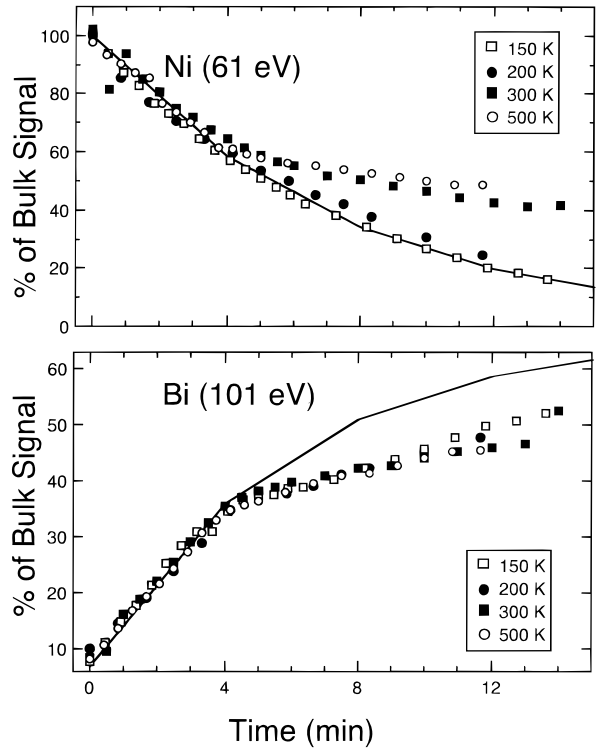

Figure 2. AES intensities during Bi deposition on Ni(100) at several temperatures. The solid lines on the graphs are for layer-by-layer growth as calculated by using the AES intensities at $\Theta_{Bi} = 1$ at 150 K.

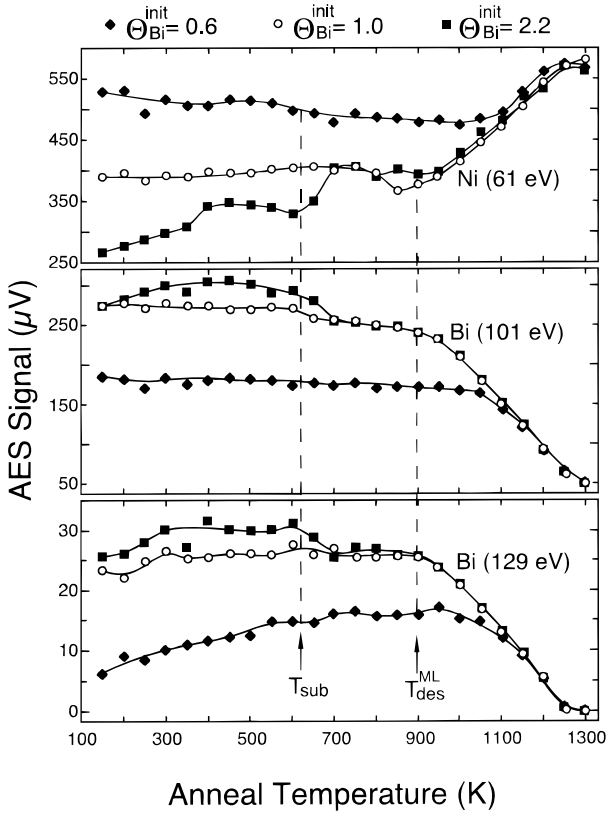

Figure 3. AES probe of the thermal stability of Ni(100) at 150 K. T_{sub} and T^{ML}_{des} indicate sublimation and monolayer-desorption temperatures, respectively, of Bi films on the Ni(100) surface.

and 600 K but remains at a value indicative of $\Theta_{Bi} > 1$. The plots of the Bi AES signals exhibit complementary and consistent behavior, showing structural changes for $\Theta_{Bi} \geq 1$ at 620 and 900 K and then decreasing toward the clean Ni signal above 900 K.

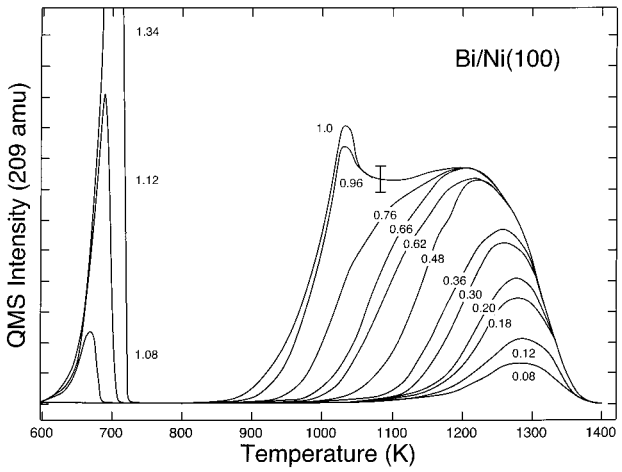

Figure 4. Bi TPD spectra after Bi deposition on Ni(100). Bi coverages (Θ_{Bi}) are given in the figure. The heating rate was 5.5 K s^{-1}.

These data indicate that the Bi monolayer is stable on Ni(100) from 150 to 900 K. Submonolayer coverages of Bi are thermally stable to even higher temperatures. The low-temperature changes observed in the substrate signal for $\Theta^{init}_{Bi} = 2.2$ can be explained by clustering and 3D Bi-island formation once sufficient thermal energy is available. These plots indicate that the 3D Bi structures that are formed for $\Theta^{init}_{Bi} = 2.2$ at 400 K are stable to 600 K. The melting point of bulk Bi is 545 K, but no particular feature was observed to correlate with that specific temperature.

As a final point about the AES spectra, which is also relevant to the plots in Figure 3, the peak shapes and positions of the Bi and Ni AES signals were not detectably changed by changing the Bi coverage. This is also supporting evidence that only small changes in the electronic structure of the Ni substrate and deposited Bi occur upon Bi adsorption relative to the bulk materials.

Bi TPD Studies. Bismuth thermally desorbs from the Ni(100) surface over the temperature range 600−1400 K as shown in Figure 4. This is consistent with our previous report.[14] The Bi TPD spectrum is characterized by two distinct desorption states. The first state filled during deposition is the Bi monolayer state, which desorbs over the range 850−1400 K. At higher Bi coverages, a Bi multilayer state desorbs at ∼650 K. The TPD spectra clearly indicate that heating to 750 K will remove only the multilayer and leave the monolayer coverage unchanged. No Ni desorption was ever observed.

The nature of the desorbing Bi species cannot be unambiguously determined by monitoring only mass 209, since the Bi atom, Bi_2 dimer, and Bi_4 tetramer all give signals at this mass. The mass resolution of the spectrometer we used precludes direct detection of species more massive than Bi atoms. Plots of Bi TPD peak area versus deposition time are linear for all coverages up to $\Theta_{Bi} = 30$ ML, but this cannot be used to determine the identity of the desorbing species because of unfavorable cross sections for electron impact ionization to produce Bi^+ from molecular species. Desorption from bulk Bi samples is known to produce high percentages of molecular species.[14,24]

The shape of the multilayer Bi desorption curves in Figure 4 is indicative of zero-order kinetics. An Arrhenius plot of these curves yields an activation energy of desorption, E_d, of 200 ± 8 kJ mol^{-1}, which gives $\Delta H_d = 205$ kJ mol^{-1},[25] in good agreement with the heat of sublimation of pure Bi, $\Delta H^\circ_{298} = 207$ kJ mol^{-1}.[24]

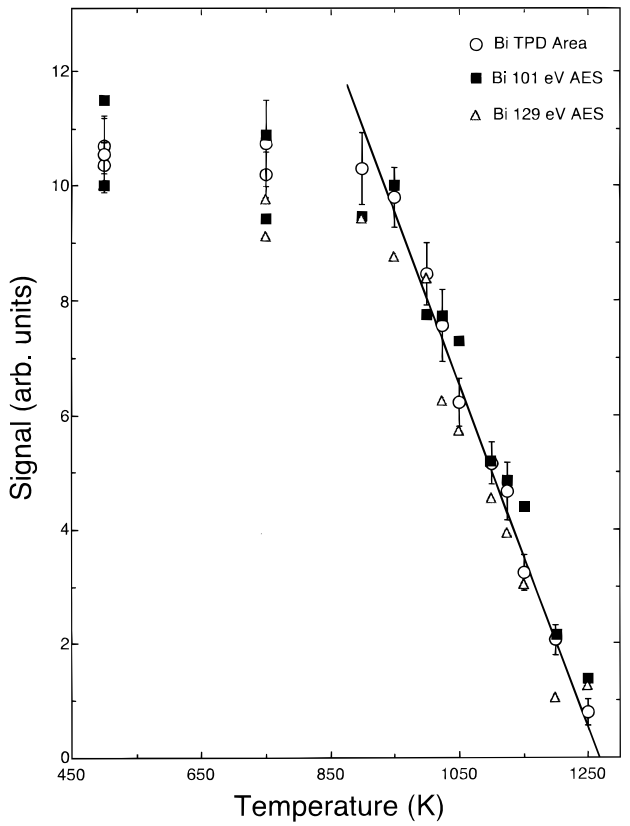

Figure 5. AES signal intensities and Bi TPD peak areas after annealing the deposited Bi layers to higher temperature.

Observations of the shapes of the desorption curves and shifts of the desorption rate maxima with Bi coverage can be used to begin analysis of the desorption kinetics of Bi coverages below one monolayer. The Bi TPD peak temperature was fairly constant for $\Theta_{Bi} < 0.2$. At these low initial coverages of Bi, the constant peak temperature with increasing coverage and the shape of the peak are indicative of first-order Bi desorption kinetics. As the coverage is increased above $\Theta_{Bi} = 0.2$, the peak begins a dramatic shift toward lower temperatures and the shape of the peak becomes irregular. The low-coverage desorption spectra can be simulated using first-order desorption kinetics with a constant value of E_d and preexponential (ν_1). This analysis produced values of $E_d = 293 \pm 16$ kJ mol^{-1} and $\nu_1 = 7.5 \times 10^{10\pm1}$ s^{-1}, assuming an order of reaction, n, of unity. If one is constrained to keep first-order desorption kinetics, then the observed shift of the desorption peak maximum to lower temperatures can only be simulated by decreasing E_d and/or increasing ν_1 as the Bi coverage increases.[26] Most likely, E_d decreases strongly near monolayer coverage because of an appreciable decrease in the Bi−Ni bond energy.

We carried out a series of annealing studies of multilayer Bi films prior to TPD analysis in order to be able to directly compare the TPD and AES results. This comparison is shown in Figure 5. The Bi TPD area was found to decrease linearly beginning at ~900 K. Bi AES intensities extracted from Figure 3 are also plotted in Figure 5. The agreement between the AES and TPD data indicates that diffusion of Bi into the bulk of Ni(100) crystal prior to Bi desorption is not an important process. If diffusion of Bi into the subsurface were prevalent in the submonolayer region, below the onset of desorption, the AES signals would decrease faster than Bi TPD areas with increasing annealing temperature. The data presented in Figure 5 also confirm that submonolayer Bi coverages can be easily and reliably prepared by annealing larger initial Bi coverages to high temperatures.

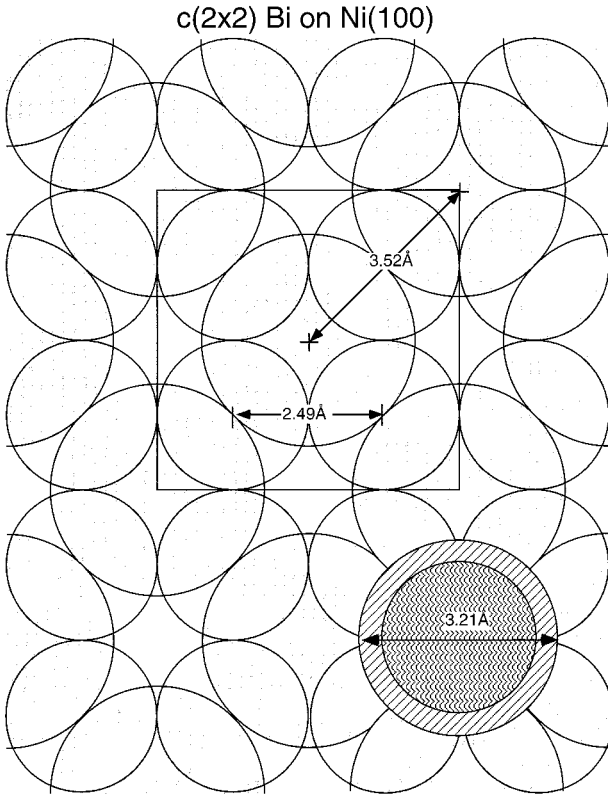

Figure 6. Real space model for the two-dimensional $c(2 \times 2)$ Bi adlayer on Ni(100) at monolayer Bi coverage. Both Ni and Bi atoms are drawn with metallic radii. The circle in the lower right-hand side indicates the single "upright" CO molecule bonded perpendicular to the surface plane according to the van der Waals radii of CO gas.

LEED Studies. LEED observations were made as a function of Bi deposition time on Ni(100) at 500 K. The only pattern observed was due to a $c(2 \times 2)$ structure. This first appeared at a coverage slightly lower than $\Theta_{Bi}^{init} = 0.5$ and persists to $\Theta_{Bi}^{init} \approx 3$. We used the LEED observations to establish an absolute surface coverage for the Bi monolayer (a structure that is only one Bi atom thick). The size mismatch between Bi and Ni atoms results in a Bi monolayer with only one-half the surface atom density of the Ni(100) substrate. The $c(2 \times 2)$ adlayer structure shown in Figure 6 is defined as the Bi monolayer, $\Theta_{Bi} = 1$, corresponding to 8.05×10^{14} atoms/cm^2. This is consistent with the value determined by RBS.[7] Continued Bi dosing above $\Theta_{Bi}^{init} = 0.5$ reduced the contrast of the pattern and increased the background intensity. The $c(2 \times 2)$ pattern began to develop diffuse streaks between the primary spots at Bi doses higher than 0.5, and finally, the primary spots were lost and only a diffuse background was observed. Warming multilayers of Bi to 750 K resulted in a sharp $c(2 \times 2)$ pattern. A $p(2 \times 2)$ structure was never observed.

UPS Studies. He(I) UPS spectra obtained for several Bi coverages on Ni(100) at 500 K are shown in Figure 7. The clean Ni(100) spectrum is characterized by strong emission within 3 eV of the Fermi energy (E_F) due to the Ni d bands, in good agreement with other published spectra.[27] The sharp feature in the clean Ni(100) spectrum near E_F is from a surface state. No new peaks due to Bi-induced states or Bi-derived states were observed within 5 eV of E_F. The attenuation of the surface state is consistent with the formation of a laterally dispersed monolayer of Bi, and the absence of new states indicates that little rehybridization of Ni was induced by Bi adsorption.

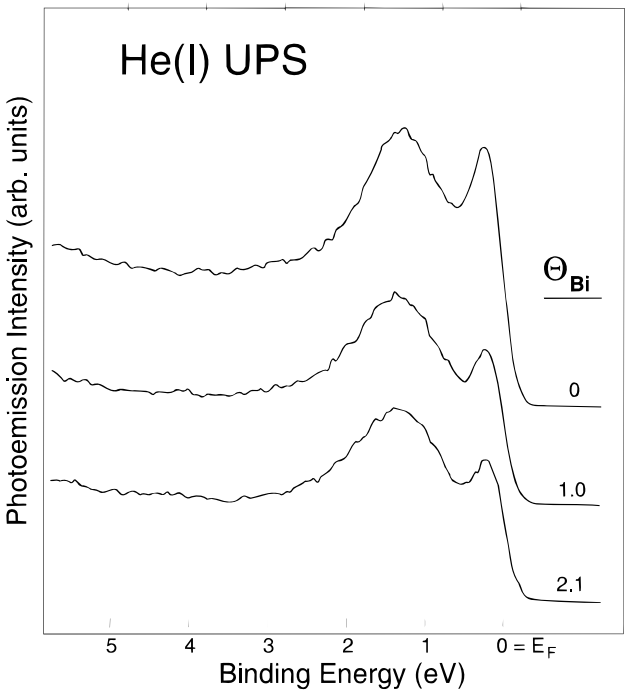

Figure 7. He(I) UPS spectra of Bi adlayers on Ni(100) 500 K.

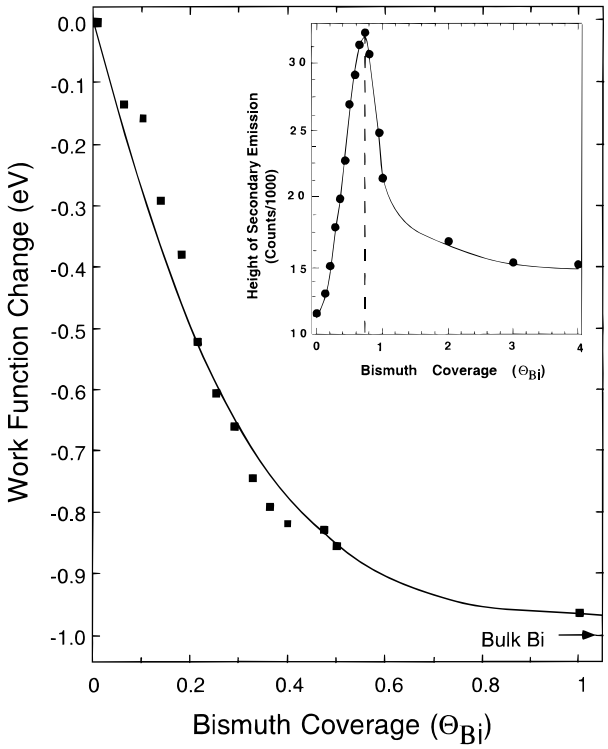

Figure 8. Change in work function induced by Bi adlayers on Ni(100) at 500 K. Values of $\Delta\phi$ were obtained from UPS spectra. The solid curve is a fit to the data using a simple point-dipole depolarization model. The inset shows how the maximum intensity of secondary electron emission varies with Bi coverage on Ni(100) at 500 K.

UPS measurements also enabled us to determine changes in the work function ($\Delta\phi$) and secondary electron emission intensity that result from Bi deposition. The work function was measured by using the onset energy for secondary electron emission. Data for $\Delta\phi$ after Bi deposition on Ni(100) at 500 K are shown in Figure 8. The decrease in ϕ with increasing Bi coverage would typically be used to infer that Bi donated electron density to the Ni substrate, but the Pauling electronegativities of Bi (1.9) and Ni (1.8)[28] predicts charge transfer from Ni to Bi.

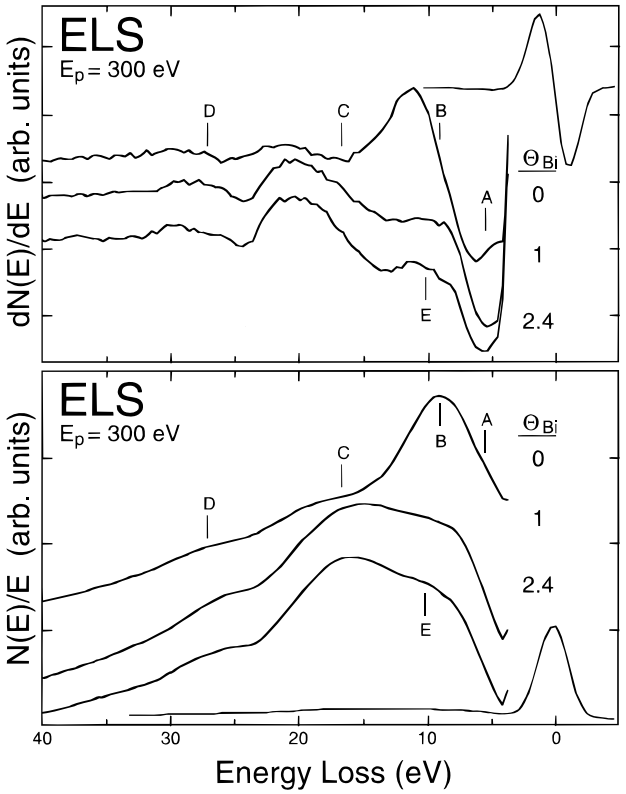

Figure 9. $N'(E)$ (top) and $N''(E)$ (bottom) ELS spectra for Bi adlayers on Ni(100) at 500 K.

The initial drop of the curve in Figure 8 at low Θ_{Bi} can be modeled using the point dipole depolarization in the classical Helmholtz model.[29,30] This yields an initial dipole moment of -0.49 D ($\pm 12\%$) and polarizability $\alpha = 4.5 \times 10^{23}$ cm^3 ($\pm 30\%$). The value of the dipole moment can be used to calculate the degree of electron withdrawal if the bond length is known. Assuming a bond distance of 3 Å[20] for the Bi−Ni bond yields a partial positive charge of only 0.03*e* on Bi.

The intensity of secondary electron emission can be useful in detecting changes in adsorbate structure,[31] and a plot of the maximum intensity of secondary electron emission for Bi deposition on Ni(100) at 500 K is shown as an inset to Figure 8. The curve increases from the value for clean Ni(100) to a peak at $\Theta_{Bi} = 0.7$ and then decreases asymptotically, approaching the value for thick Bi films. The peak is indicative of some change in the surface structure, and we ascribe this to nucleation of $c(2 \times 2)$ Bi islands near $\Theta_{Bi} = 0.7$ and completion of the $c(2 \times 2)$ structure near $\Theta_{Bi} = 1$.

ELS Studies. ELS spectra at $E_p = 300$ eV from Bi adlayers on Ni(100) at 500 K are shown in Figure 9. Assignments for clean Ni(100) were taken from previous work.[32,33] Peak A is a combination of several low-energy interband transitions and is not influenced by deposited Bi adatoms. Peak B is due to a Ni surface plasmon and is greatly attenuated by adsorbed Bi. The peaks labeled C and D are assigned as Ni volume plasmons and are affected only slightly by Bi deposition. The small feature labeled E, which is present only at high Bi coverage, is assigned to a Bi plasmon,[34] and the additional intensity in peak C with increasing Bi coverage is assigned to the surface plasmon of the overlayer structure.

3.2. CO Chemisorption. *TPD Studies.* CO TPD spectra following saturation coverages of CO on clean Ni(100) and Bi-

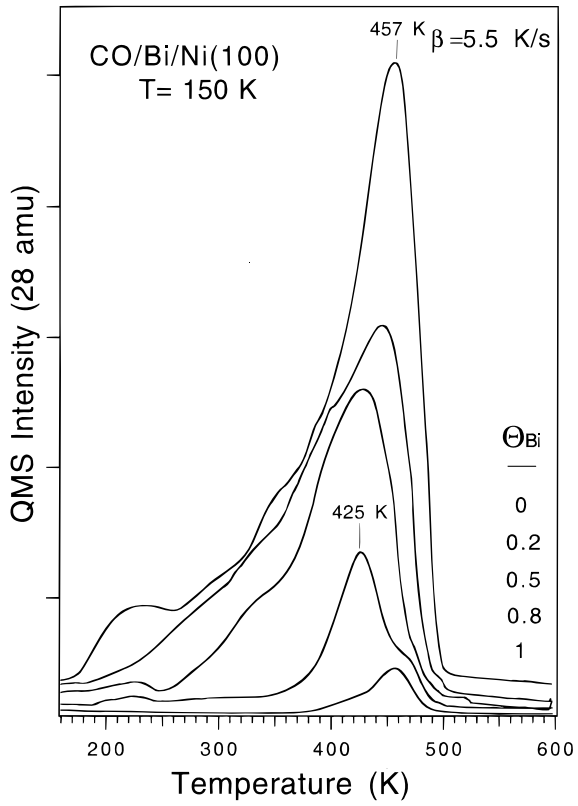

Figure 10. CO thermal desorption spectra probing the effects of preadsorbed Bi on CO coverage and binding energy on Ni(100) at 150 K.

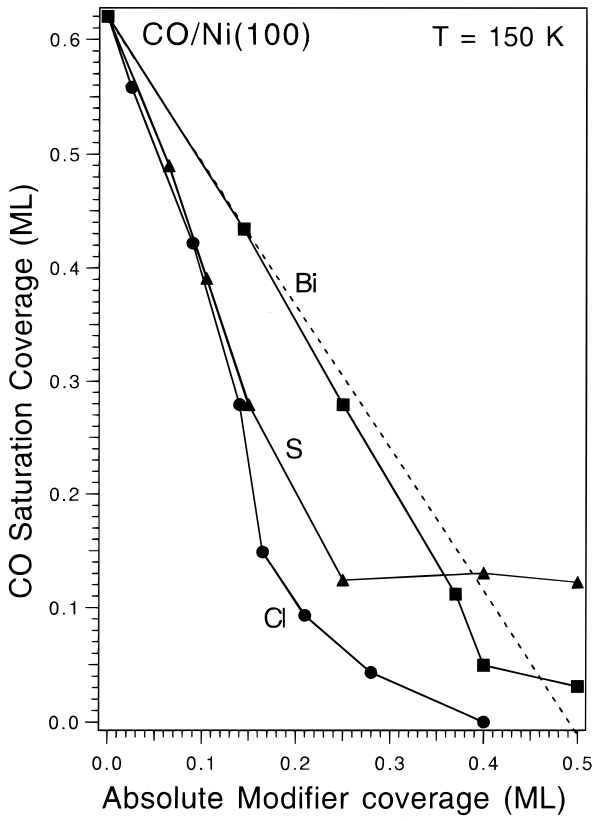

Figure 11. Comparison of the effectiveness of several adatom modifiers to reduce the CO saturation coverage on Ni(100) at 150 K. Data for the S and Cl adatoms were taken from ref 39. The dashed line predicts the theoretical variation of Θ_{Bi} according to the relationship $\Theta_{CO}^{mod} = \Theta_{CO}^{sat}(1 - 2\Theta)$.

precovered Ni(100) surfaces at 150 K are shown in Figure 10. The thermal desorption spectrum of CO adsorbed on the clean Ni(100) surface is in good agreement with results from previous studies.[35,36] Desorption of CO from Ni(100) exhibits one high-temperature peak near 460 K and a broad profile down to 180 K because of CO−CO repulsive lateral interactions.[37] Precovering the Ni(100) surface with Bi adatoms caused the low-temperature, broad features to disappear and suppressed the CO peak at 460 K. The general decrease in the amount of CO chemisorption is expected because of site-blocking effects of the Bi adlayer on Ni(100). A small (40 K) shift in the CO desorption peak temperature also occurred with increasing Θ_{Bi}. Islands of the $c(2 \times 2)$Bi/Ni(100) structure exists for $\Theta_{Bi} > 0.5$, and CO adsorption is essentially eliminated for $\Theta_{Bi} > 0.8$. The small amount of CO desorption for $\Theta_{Bi} = 1.0$ is probably from domain boundaries or other defects in the Bi adlayer that provide some additional access to the Ni substrate.

Redhead analysis[38] using CO TPD peak maxima and $\nu_1 = 10^{14}$ s^{-1} indicates that the CO desorption energy of the most strongly chemisorbed species decreases about 10 kJ mol^{-1} from 117 kJ mol^{-1} on Ni(100) to 107 kJ mol^{-1} when $\Theta_{Bi} = 0.8$.

Figure 11 shows the influence of preadsorbed Bi upon the saturation coverage in a monolayer of CO on Ni(100) at 150 K. Similar data[39] reported for the electronegative adatoms Cl and S are also shown for comparison. The CO monolayer coverage decreased linearly with Θ_{Bi}, and CO adsorption was effectively suppressed at 0.4 ML (absolute coverage). The dashed line represents a simulation according to the relationship $\Theta_{CO}^{mod} = \Theta_{CO}^{sat}(1 - 2\Theta)$. This assumes that each Bi atom blocks two Ni atoms and that the CO adsorption site is a single Ni atom.

The initial sticking coefficient of CO on these same chemically modified Ni(100) surfaces at 150 K is shown in Figure 12. For small Bi coverages, S_0 does not decrease as fast as might be expected from simple Langmuirian adsorption in the presence of a site blocker. The dashed line describes the adsorption kinetics expected if $S_0^{mod} = S_0(1 - 2\Theta)$, again assuming each Bi atom blocks two Ni atoms and CO adsorption requires only one Ni atom. The deviation from the dashed line is because of the importance of the modifier precursor adsorption state.[40] However, for preadsorbed S and Cl adatoms, electronic effects additionally influence CO adsorption kinetics. The effect of Bi adatoms reducing both Θ_{CO} and S_0 for CO adsorption on Ni(100) is much smaller than that for Cl and S adatoms at the same modifier precoverages.

CO HREELS Studies. Vibrational studies show that the adsorption sites of CO on Ni(100) depend on both surface temperature and coverage.[41−43] At low temperatures, CO predominantly adsorbs on bridge sites at low coverages and then populates atop sites. However, at room temperature, the atop sites are predominantly occupied even at low coverages.

The influence of preadsorbed Bi adatoms on the population of CO adsorption sites after large (saturation) CO exposures on Ni(100) at 150 K is shown in Figure 13. On clean Ni(100), CO is mainly adsorbed on bridge sites with ν_{CO} at 1986 cm^{-1}, which is consistent with previous results.[42,43] With increasing coverage of Bi adatoms on the Ni(100) surface, the dominant loss peak at 1986 cm^{-1} shifted downward in frequency by ~60 cm^{-1} to about 1920 cm^{-1} for $\Theta_{Bi} = 0.4$, as might be expected from decreased CO−CO lateral interactions because of lower CO coverages on these surfaces. On clean Ni(100), a 40 cm^{-1} shift to lower energy is observed as the CO coverage is reduced from saturation to a small value.[41,42] The large shift (~180 cm^{-1}) in ν_{CO} for $\Theta_{Bi} = 0.74$ is likely to be associated with a new

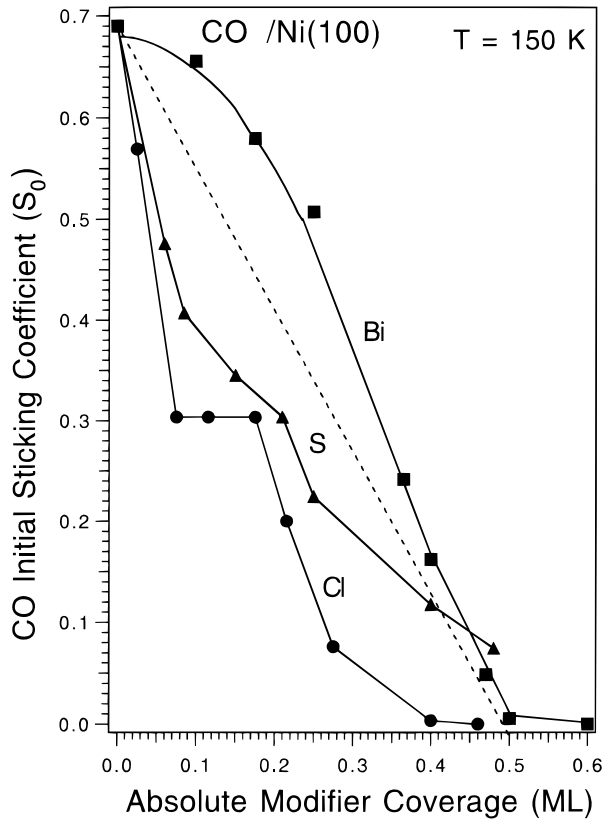

Figure 12. Influence of several preadsorbed adatoms on the CO initial sticking coefficient on Ni(100). The dashed line shows variation of S_0 according to the relationship $S_0^{mod} = S_0(1 - 2\Theta)$.

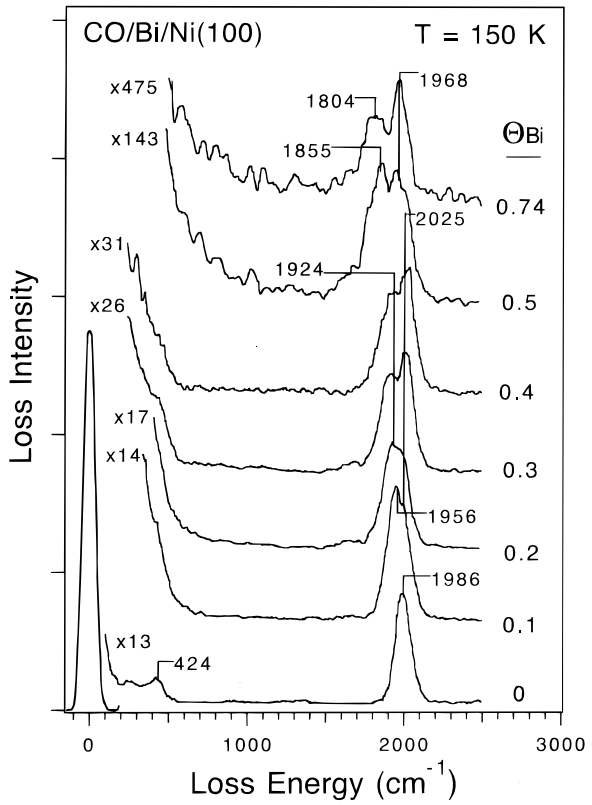

Figure 13. HREELS spectra after saturation doses of CO on Bi-precovered Ni(100) surfaces at 150 K.

peak at smaller loss energy. At a Bi precoverage of $\Theta_{Bi} \geq 0.1$, a new loss peak appeared at 2025 cm^{-1} and the intensity of this peak increased to $\Theta_{Bi} = 0.4$. This peak also shifted downward by ~60 cm^{-1} to 1968 cm^{-1} at higher Bi coverages.

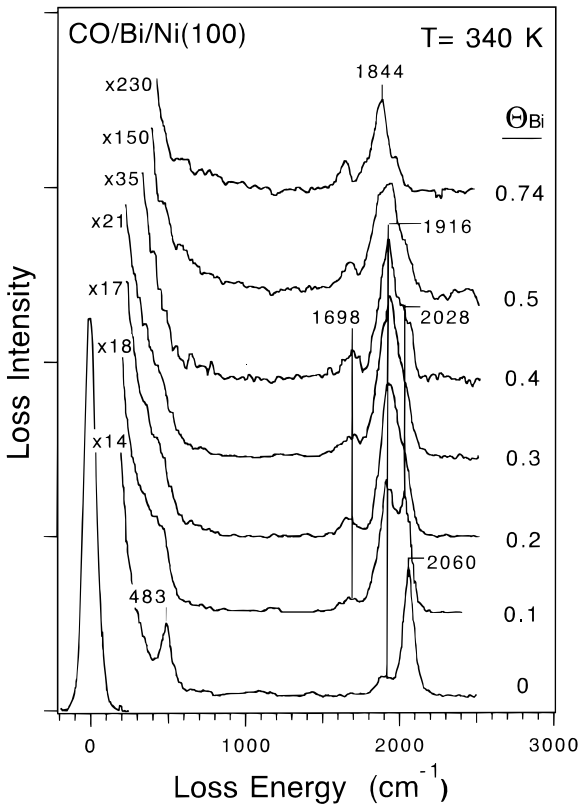

Figure 14. HREELS spectra after saturation doses of CO on Bi-precovered Ni(100) surfaces at 340 K.

HREELS spectra of saturation coverages of CO on Ni(100) and Bi-precovered Ni(100) surfaces at 340 K are shown in Figure 14. The dominant ν_{CO} loss peak is at 2060 cm^{-1} on clean Ni(100) at 340 K, and hence, CO is predominantly adsorbed at atop sites. The smaller loss peak at 1916 cm^{-1} is assigned to bridge-bonded CO. The loss peak at 2060 cm^{-1} shifted to 2028 cm^{-1}, and the intensity of this peak decreased at $\Theta_{Bi} = 0.20$. This peak almost completely disappeared at $\Theta_{Bi} = 0.4$, and also the ν_{CO} intensity for bridge-bonded CO increased. Bi adsorption also caused a new peak at 1698 cm^{-1} to appear. The absence of a significant shift in ν_{CO} for both atop and bridge-bonded CO is consistent with the TPD results and shows that Bi does not have a substantial electronic effect on the Ni(100) substrate and that a site-blocking effect is dominant.

4. Discussion

AES intensity measurements as a function of Bi evaporation time are modeled well by FM-growth simulation curves for Bi deposition on Ni(100) at 150 K. However, it is most likely that Bi forms metastable, supersaturation structures.[18] At low temperatures, Bi adatoms do not have sufficient thermal energy to aggregate into 3D islands and simply stick at positions where they collide with the surface. As the deposition temperature is raised, the thermodynamically favored 3D structures are formed as the Bi mobility increases.

For Bi deposition on Ni(100) at 500 K, a Stranski−Krastanov (SK) growth mode of Bi on Ni(100) is followed, i.e., the growth of 3D Bi crystallites on top of the first Bi monolayer. Even though such AES curves can also be indicative of the formation of surface alloys,[44] the surface free energy of Bi (382 mJ m^{-2}) is much lower than that of Ni (2364 mJ m^{-2}),[45] and this suggests

that formation of Bi layers would be preferable to diffusion into the bulk. Also, the solubility of Bi in Ni is known to be small.[46] The large difference in surface free energies indicates that formation of a stable 2D monolayer structure should be favored over immediate formation of 3D crystallites. The agreement between AES and TPD annealing results provides evidence that diffusion of Bi deep into the bulk is not an important process. Further evidence for a SK growth mode is given by the ELS data. The immediate loss of the Ni(100) surface plasmon after Bi deposition indicates that the adsorbate does not form localized islands or 3D crystallites at low Bi coverages. If islands did occur, then the substrate surface plasmon would persist and appear with the bulk plasmon of the overlayer structure.[47] The immediate loss of the surface plasmon indicates that a stable monolayer structure is formed prior to any 3D growth. On the basis of all of these results, we conclude that Bi films nucleate and grow in a SK fashion on Ni(100) at 500 K. An SK growth mode was also observed for Bi films on Pt(111) at 600 K [5] and in the related system of Pd on Ni(100) at 300 K.[48,49] However, a disordered Bi/Cu surface alloy was formed on Cu(100) at 300 K up to about $\Theta_{Bi} = 0.35$.[9]

Bi forms an ordered $c(2 \times 2)$ structure with a LEED pattern that fades as Bi forms close-packed layers in thicker films that are incommensurate with the Ni substrate. The diffuse background, which forms with increasing Bi deposition, is consistent with a disordered structure caused by the formation of 3D crystallites. The conversion of diffuse spots to streaks at higher Bi coverages is analogous to those observed for Bi on Cu(100)[9] and Pb on Ni(100).[48] These were attributed to hexagonal crystallites such as $c(n\sqrt{2} \times \sqrt{2})$R45° ($n = 9, 7, 5$, respectively) formed over the fcc substrate lattice.[9,48]

The presence of $c(2 \times 2)$ spots in LEED at coverages below $\Theta_{Bi} = 1$ indicates that there are attractive lateral interactions between Bi adatoms. However, these are insufficient to cause earlier (lower coverage) nucleation of the $c(2 \times 2)$ structure or condensation into more compact arrangements. Primarily the energetics of the Bi−Ni bond determine the monolayer structure. Bi TPD spectra show that the Bi adsorption energy decreases with increasing Bi coverages, and this provides the thermodynamic driving force for spreading Bi atoms on Ni(100) substrate. A $p(2 \times 2)$ structure was never observed. The $p(2 \times 2)$ structure would be expected to form at $\Theta_{Bi} = 0.5$ if strong lateral repulsive interactions existed.

The effect of different modifiers (chemisorbed as adatoms) on the work function of Ni(100) is shown in Figure 15. It is evident that electrostatic interactions of Bi adatoms with the Ni substrate are much weaker than that for alkali metal adatoms. The absence of a pronounced minimum in the Bi curve is a reflection of significantly less mutual depolarization in the Bi adlayer than that found for alkali metals. The dipole moment that can be ascribed to Bi adatoms of 0.49 D is near that for Xe (0.30 D) on Ni(100).[30] This is consistent with UPS spectra showing little perturbation of Ni(100) states by Bi adatoms. The reduction in work function at low Bi coverage is usually assigned to some charge transfer from Bi to Ni, as in the case on Pt(111).[5] Dipole−dipole repulsive interactions can cause adatom lateral repulsion, but the presence of small dipoles means that there is only a weak lateral repulsion between Bi adatoms. A direct comparison to the Bi/Pt(111) system, as shown in Figure 16, reveals that the value of $\Delta\phi$ associated with the Bi monolayer ($\Delta\phi = 1$ eV) on Ni(100) is smaller than that found on Pt(111) ($\Delta\phi = 2$ eV).[5]

The addition of Bi adatoms on Ni(100) significantly reduces the total amount of CO adsorption at 150 K on the surface.

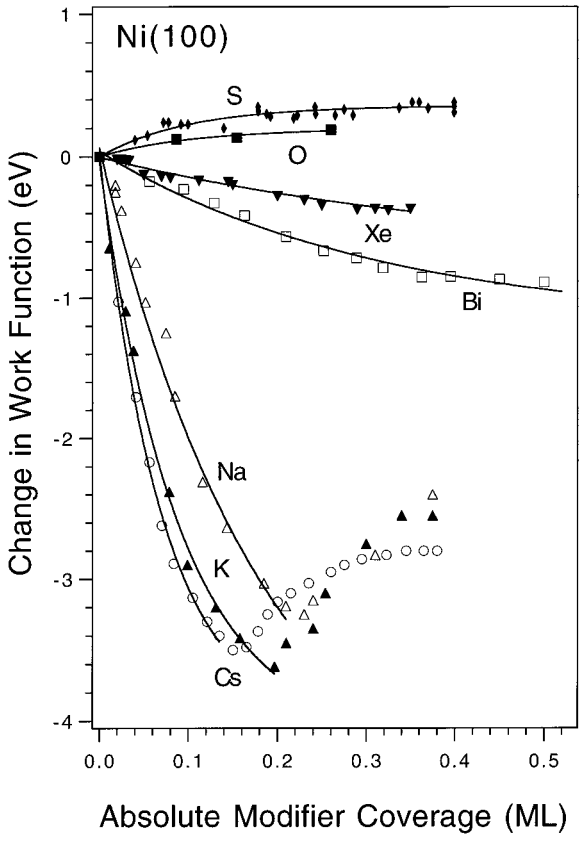

Figure 15. Work function change on chemically modified Ni(100) surfaces for several different adatom modifiers on the surface.

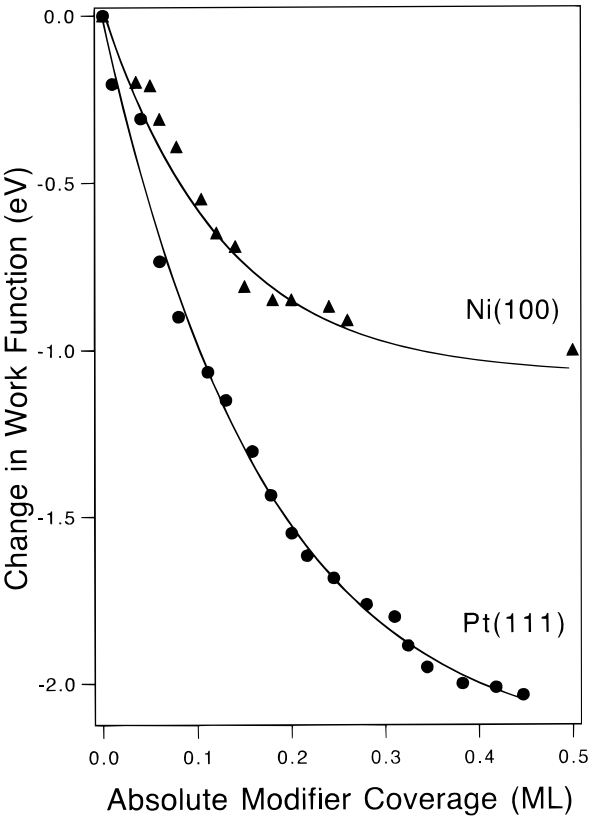

Figure 16. Comparison of the work function change due to Bi adsorption on Pt(111) and Ni(100) surfaces.

Weakly bound CO, which desorbs in the low-temperature TPD peaks on Ni(100), is preferentially reduced at low Θ_{Bi}. Significantly, there is relatively little change in the CO desorp-

tion peak temperature that corresponds to the most strongly adsorbed CO throughout the entire range of Bi coverage. Thus, the poisoning of CO adsorption on the surface occurs as a result of a short-range, site-blocking influence by Bi adatoms on the Ni(100) surface. CO adsorption is nearly completely blocked by a $c(2 \times 2)$ Bi monolayer. Because there are no significant electronic effects on the Ni(100) substrate due to coadsorbed Bi, the changes in CO adsorption and desorption behavior with increasing Θ_{Bi} are close to that of changing CO coverages on clean Ni(100), i.e., CO−Bi repulsive interactions within the coadsorbed layer are similar to those of CO−CO repulsive interaction with the CO adlayer at high CO coverages on clean Ni(100).

A local site-blocking effect of Bi is also indicated by the observed linear decrease of the CO saturation coverage with increasing Θ_{Bi} in Figure 11. The same kind of linear relationship was observed for CO on Bi/Pt(111) surfaces.[10] The influence of Bi precoverage on CO adsorption on Ni(100) can be described by $\Theta_{CO}^{mod} = \Theta_{CO}^{sat}(1 - 2\Theta)$; i.e., each Bi adatom blocks two Ni atoms and only one Ni atom is required for a CO chemisorption site. A comparison of the suppression of CO adsorption by Bi adatoms to that of the electronegative adatoms Cl and S is shown in Figures 11 and 12. Bi has much less affect on CO adsorption kinetics and chemisorption coverages than Cl or S adatoms. This can be explained by the additional changes in the electronic structure at Ni surface atoms due to the presence of these electronegative adatoms.[39] The increased influence of S adatoms over that of Cl adatoms on CO adsorption has the same trend as the electronegativity of the preadsorbed atoms. This is also consistent with a minimal electronic perturbation of Ni by Bi adatoms.

In CO adsorption studies on Bi/Pt(111) surfaces,[10] Bi adatoms were used as a "model" system for the effect of inert site blockers. Bi adatoms in that case influenced CO chemisorption more strongly than for the case of Ni(100) here. For CO/Bi/Pt(111), there was a shift of the CO TPD peak to lower temperatures and a narrowing of the peaks such that E_d decreased from 112 kJ mol^{-1} on Pt(111) to 106 kJ mol^{-1} for $\Theta_{Bi} = 0.25$. E_d then increased back to near the CO/Pt(111) value near $\Theta_{Bi} = 0.62$, where the CO chemisorption was completely suppressed. Bi also altered the population of CO adsorption sites on Pt(111), assuming constant dynamic dipoles. There was an increased population of bridge-bonded CO for a given total coverage of CO, and also there was a large (200 cm^{-1}) shift in ν_{CO} to lower energy for bridge-bonded CO on Bi/Pt(111) surfaces. Bi and CO are probably present in an intermixed adlayer on Pt(111), and the decreased adsorption energy and the increased population in bridging sites with increasing Bi precoverages are likely due to CO−Bi repulsive interactions.[10] In light of our results on Ni(100), it could also be that a small electronic effect of Bi on Pt(111) contributes or causes the large shift in ν_{CO} at high Bi coverages for CO/Bi/Pt(111).

Vibrational data for CO/Bi/Ni(100) at 150 K further confirms that local interactions are dominant. The loss peaks at 2025 and 1986 cm^{-1} for clean Ni(100) can be assigned as atop and bridge-bonded CO, respectively, on the Ni(100) surface.[41−43] The gradual downward shift of ∼60 cm^{-1} in the CO stretching frequencies for both the atop CO and bridge-bonded CO can be explained by the removal of the CO−CO dipole coupling via screening by the coadsorbed Bi adatoms. However, the very large apparent shift (∼180 cm^{-1}) for bridge-bonded CO is most likely due to the presence of unresolved peaks for CO in both 2-fold bridge sites (∼1900 cm^{-1}) and newly populated 4-fold hollow sites (∼1700 cm^{-1}). CO adsorbed on 4-fold hollow sites with a loss peak at 1740 cm^{-1} was also observed on a S-precovered Ni(100) surface at high S adatom coverages.[50]

When CO was adsorbed at 340 K, there was an increase in the population of bridge-bonded CO relative to that of atop CO. Also, a new ν_{CO} band appeared at 1698 cm^{-1} that can be assigned to CO adsorbed at 4-fold hollow sites on Ni(100).[50] The relatively large population of bridge-bonded CO at higher Bi coverages could be due to more extensive CO−Bi repulsive interactions that arise in a more extensively intermixed layer of CO and Bi at 340 K compared to more segregated domains of two different phases at 150 K. The elimination of atop CO bonding sites is a natural consequence of the large size of Bi adatoms and the preference of Bi to bond at 4-fold hollow sites.

5. Conclusion

New, complementary information was gained about Bi adlayers deposited on Ni(100). Bi films grow on Ni(100) at 500 K by first forming a $c(2 \times 2)$-Bi monolayer structure and then 3D Bi islands. Bi desorbs from the monolayer over a temperature range ∼850−1350 K because of strong Bi−Bi repulsive interactions at high Θ_{Bi}. Multilayers of Bi desorb with near-zero-order kinetics near 600 K with an activation energy of 200 ± 8 kJ mol^{-1}, in good agreement with the bulk heat of sublimation. Modification of the electronic structure of the Ni substrate by Bi adatoms is minimal. Within a point dipole model for work function changes, no significant electron transfer occurs between Bi and Ni.

The influence of Bi adatoms on Ni(100) chemistry was probed by CO adsorption. CO chemisorption on Ni(100) was poisoned by Bi adatoms, with a linear decrease in CO coverage with Θ_{Bi} and nearly complete blocking of CO chemisorption at $\Theta_{Bi} = 1.0$. TPD and HREELS spectra obtained for CO adsorbed on Bi-precovered Ni(100) surfaces were only slightly modified. This indicates a minimal electronic influence of Bi adatoms on Ni(100) substrate. HREELS shows an increased population of CO adsorbed at atop sites at low temperature (150 K), whereas Bi adatoms force CO to adsorb mainly at 2-fold bridge sites with some population of 4-fold hollow sites at 340 K.

The combination of the propensity to form a dispersed adlayer at low Θ_{Bi} and the minor electronic perturbations due to Bi−Ni bonding suggests that Bi adatoms will allow further probing of the constraints that modifier adatoms impose on adsorption and reaction ensemble requirements on Ni(100) surface.

Acknowledgment. Support from the U.S. Department of Energy, Office of Basic Energy Sciences, Chemical Sciences Division is gratefully acknowledged. We also thank Randall J. Smith for his contributions to this work.

References and Notes

(1) Briner, B. G.; Feenstra, R. M.; Chin, T. P.; Woodall, J. M. *Phys. Rev. B* **1996**, *54*, R5283.

(2) Patrin, J. C.; Li, Y. Z.; Chander, M.; Weaver, J. H. *J. Vac. Sci. Technol. A* **1993**, *11*, 2073.

(3) Kaigawa, R.; Sakaguchi, T.; Herrmann, R.; Kaito, C.; Miki, H.; Nakayama, Y. *J. Mater. Sci.* **1995**, *30*, 2348.

(4) Chakoumakos, B. C.; Ebey, P. S.; Sales, B. C.; Sonder, E. *J. Mater. Res.* **1989**, *4*, 767.

(5) Paffett, M. T.; Campbell, C. T.; Taylor, T. N. *J. Chem. Phys.* **1986**, *85*, 6176.

(6) Puckrin, E.; Slavin, J. A. *Phys. Rev. B* **1990**, *41*, 4970.

(7) Klink, C.; Foss, M.; Stensgaard, I.; Besenbacher, F. *Surf. Sci.* **1991**, *251/252*, 841.

(8) Godfrey, D. C.; Hayden, B. E.; Murray, A. J.; Parsons, R.; Pegg, D. J. *Surf. Sci.* **1993**, *294*, 33.

(9) Meyerheim, H. L.; Zajonz, H.; Moritz, W.; Robinson, I. K. *Surf. Sci.* **1997**, *381*, L551.

(10) Paffett, M. T.; Campbell, C. T.; Windham, R. G.; Koel, B. E. *Surf. Sci*. **1989**, *207*, 274.
(11) Henn, F. C.; Dalton, P. J.; Campbell, C. T. *J. Phys. Chem*. **1989**, *93*, 836.
(12) Sachtler, W. M. H. *Handbook of Catalysis*, to be published.
(13) Sachtler, J. W. A.; Somorjai, G. A. *J. Catal*. **1983**, *81*, 77.
(14) Jones, M. E.; Heitzinger, J. M.; Smith, R. J.; Koel, B. E. *J. Vac. Sci. Technol. A* **1990**, *8*, 2512.
(15) Windham, R. G.; Bartram, M. E.; Koel, B. E. *J. Phys. Chem*. **1988**, *92*, 2862.
(16) Coghlan, W. A.; Clausing, R. E. *At. Data* **1973**, *5*, 317.
(17) Jackson, D. C.; Gallon, T. E.; Chambers, A. *Surf. Sci*. **1973**, *36*, 381.
(18) Venables, J. A.; Spiller, G. D. T.; Hanbucken, M. *Rep. Prog. Phys*. **1984**, *47*, 399.
(19) Reichelt, K. *Vacuum* **1988**, *38*, 1083.
(20) Barrett, C. S. *Struct. Rep.* **1947**−**1948**, *11*, 44.
(21) Seah, M. P.; Dench, W. A. *Surf. Interface Anal*. **1979**, *1*, 2.
(22) Powell, C. J. *J. Vac. Sci. Technol. A* **1985**, *3*, 1338.
(23) Ossicini, S.; Memeo, R.; Ciccacci, F. *J. Vac. Sci. Technol. A* 1**985**, *3*, 387.
(24) Kohl, F. J.; Uy, O. M.; Carlson, K. D. *J. Chem. Phys*. **1967**, *47*, 2667.
(25) $\Delta H = \Delta E + \Delta(PV) \approx \Delta E + \Delta nRT$.
(26) Zhandov, V. P. *Surf. Sci*. **1983**, *133*, 469.
(27) Koel, B. E.; Peebles, D. E.; White, J. M. *Surf. Sci*. **1983**, *125*, 709.
(28) Pauling, L. *The Nature of the Chemical Bond*, 3rd ed.; Cornell University: Ithaca, NY, 1960.
(29) Albano, E. V. *Appl. Surf. Sci*. **1983**, *14*, 183.
(30) Christmann, K.; Demuth, J. E. *Surf. Sci*. **1982**, *120*, 291.
(31) Argile, C.; Barthes-Labrousse, M.-G.; Rhead, G. E. *Surf. Sci*. **1984**, *138*, 181.
(32) Montano, P. A.; Vaishnava, P. P.; Boling, E. *Surf. Sci*. **1983**, *130*, 191.
(33) Lee, Y. C.; Abu-joudeh, A.; Montano, P. A. *Surf. Sci*. **1984**, *143*, 469.
(34) Raether, H. *Excitation of Plasmons and Interband Transitions by Electrons*; Springer-Verlag: Berlin, 1980.
(35) Yates, J. T., Jr.; Goodmann, D. W. *J. Chem. Phys*. **1980**, *73*, 53.
(36) Lauterbach, J.; Wittmann, M.; Küppers, J. *Surf. Sci*. **1992**, *279*, 287.
(37) King, D. A. *CRC Crit. Rev. Solid State Sci*. **1978**, *7*, 167.
(38) Redhead, P. A. *Vacuum* **1962**, *12*, 203.
(39) Kiskinova, M.; Goodman, D. W. *Surf. Sci*. **1981**, *108*, 64.
(40) Xu, C.; Koel, B. E. *J. Phys. Chem*. **1994**, *100*, 664.
(41) Bezinger, J. B.; Schoofs, G. R. *Surf. Sci*. **1986**, *171*, L401.
(42) Lauterbach, J.; Wittmann, M.; Küppers, J. *Surf. Sci*. **1992**, *279*, 287.
(43) Yoshinobu, J.; Takagi, N.; Kawai, M. *Chem. Phys. Lett*. **1993**, *211*, 48.
(44) Rhead, G. E. *J. Vac. Sci. Technol*. **1976**, *13*, 603.
(45) Mezey, L. Z.; Giber, J. *Jpn. J. Appl. Phys*. **1982**, *21*, 1569.
(46) Nash, P. *Bull. Alloy Phase Diagrams* **1985**, *6*, 345.
(47) Bevolo, A. J. *J. Vac. Sci. Technol. A* **1985**, *3*, 1312.
(48) Gurtler, K.; Jacobi, K. *Surf. Sci*. **1985**, *152/153*, 272.
(49) Argile, C. *Surf. Sci*. **1998**, *398*, 221.
(50) Gland, J. L.; Madix, R. J.; McCabe, R. W.; DeMaggio, C. *Surf. Sci*. **1984**, *143*, 46.